Subsynchronous Control Interaction Analysis and Trigger-based Damping Control for Doubly Fed Induction Generator-based Wind Turbines

Jian Zhang, Xiangning Xiao, Peng Zhang, Jingjing Lu & Taofeek Orekan

Taylor & Francis
Taylor & Francis Group

Subsynchronous Control Interaction Analysis and Trigger-based Damping Control for Doubly Fed Induction Generator-based Wind Turbines

Jian Zhang,[1] Xiangning Xiao,[1] Peng Zhang,[2] Jingjing Lu,[1] and Taofeek Orekan[2]
[1]State Key Laboratory for Alternate Electrical Power System with Renewable Energy Sources, North China Electric Power University, Beijing, China
[2]Department of Electrical and Computer Engineering, University of Connecticut, Storrs, Connecticut, USA

CONTENTS

Abstract—Doubly fed induction generator-based wind turbines are vulnerable to subsynchronous oscillations. Subsynchronous control interaction is a recently emerging subsynchronous oscillation phenomenon, which means the interaction between the rotor-side converter of a doubly fed induction generator-based wind turbine and a fixed series-compensated transmission line. In this article, subsynchronous control interaction is quantitatively analyzed, and an subsynchronous control interaction-triggered condition is created to detect the existence of subsynchronous control interaction. The subsynchronous control interaction-triggered condition is then combined with impedance scanning to effectively identify the induction generator effect and subsynchronous control interaction. Further, a subsynchronous control interaction-triggered damping control strategy is developed to effectively alleviate subsynchronous control interaction. The mitigation ability and the robustness of the presented control strategy are, respectively, verified by time-domain simulation.

1. INTRODUCTION

Due to the economic growth and environmental concerns for traditonal power generation, renewable energies, such as photovoltaic [1], wind [2], and tide [3], have exhibited their promising benefits for the electric power industry. Among those renewables integrated into the power grid, wind power generation has so far been the top choice due to its high technical viability and energy density [4]. Since wind energy is normally generated in remote regions, in many cases, the electric power produced by wind farms has to be delivered to load centers through long-distance transmission lines. A major bottleneck of long-distance wind power delivery is the limited transmission capacity of transmission lines. To solve this problem, series capacitor compensation is widely used to improve transmission capacity by reducing the equivalent reactance of a transmission line [5]. However, as do conventional steam-turbine generators [6, 7], wind turbines also suffer from the risk of subsynchronous oscillation (SSO) when they are

713

connected radially by the fixed series-compensated transmission lines [8–11].

Unlike steam-turbine generators, the shaft stiffness of a wind turbine is generally small; thus torsional interaction (TI) is not the main SSO problem in a wind turbine. By contrast, the induction generator effect (IGE) and subsynchronous control interaction (SSCI) would affect wind turbines more seriously [12], which are not related to the shaft but determined by the resonance frequency of the power grid. In this article, the two types of SSO problems pertinent to wind generators, *i.e.*, IGE and SSCI, are referred to as non-torsional SSO. Of the four major types of wind turbines, doubly fed induction generator (DFIG) based wind turbines are most vulnerable to non-torsional SSO [13] because the stator of the induction generator is directly connected to the power grid. the SSCI is a newly discovered SSO phenomenon for wind power plants, which is primarily caused by the interaction between the rotor-side converter (RSC) of a DFIG-based wind turbine and a fixed series-compensated transmission line. In 2009, the first practical experience of SSCI in a DFIG-based wind farm occurred in the territory of the Electric Reliability Council of Texas (ERCOT). It was caused by an unplanned outage that resulted in fast-growing current and voltage oscillations and the damage of crowbar circuits [14, 15]. That event motivated relevant researchers to analyze and identify SSCI. A two-step method that combines impedance scanning and time-domain simulation to identify SSCI was introduced in [16]; however, it is quite challenging to use this method to separately observe the SSCI due to similar characteristics with IGE. Also, two kinds of steady-state models involving eigenvalue analysis were proposed to identify IGE and SSCI in [17]. The authors demonstrated inconspicuous differences between the two models, so SSCI related to the dynamic of the RSC could not be emphasized. Thus, some other methods should be further considered to separate SSCI from IGE more effectively.

On the other hand, mitigation of SSCI after detection should be taken into consideration. Mitigation methods that focus on the RSC, for example, regulating the controller parameters, adding low-pass filters, and SSCI damping control in the RSC, were introduced in [18]. However, these kinds of method may influence the main function of the controller in normal operation, since the SSCI mitigation function exists throughout even when there is no SSCI. Another method was presented in [18] that added extra devices, such as bypass filters, across the series capacitor or installing protection into the system. The disadvantage of these methods is the additional expenses. A static VAR compensator (SVC) with a damping controller was developed in [19], but like the latter method, it is costly due to the addition of extra devices. A supplemental control was introduced in the reactive power control loop of the grid-side

converter (GSC) of a DFIG-based wind turbine to solve the SSO problem in [20]. However, for the SSCI problem, which is mainly related to the RSC with higher controllability [17], the damping capability from the GSC could not be provided sufficiently, as analyzed in [21]. Hence, a two-degree-of-freedom control strategy used in the RSC was proposed in [22] to improve the IGE handing capability of the system, although its handing capability for SSCI was not analyzed in detail.

In this article, the system including a single DFIG-based wind turbine connected to a fixed series-compensated transmission line is used to analyze the SSCI. According to the analysis, an SSCI-triggered condition including the dynamic of RSC is developed to identify the existence of SSCI. The condition is combined with an impedance scanning approach to effectively separate IGE and SSCI, which is verified by time-domain simulation. A time-domain simulation is also utilized to verify the SSCI-triggered condition with different wind speeds, series compensation levels, as well as the outer and inner gains of the RSC controller. An SSCI-triggered damping control strategy is proposed and designed to mitigate SSCI effectively. The mitigation ability of the proposed control strategy is verified by time-domain simulation with the changes of wind speed and series compensation level. And the robustness and advantage compared with other methods of the method are analyzed.

This article is organized as follows. Section 2 elaborates on the SSCI phenomenon and proposes an SSCI-triggered condition. Section 3 presents a comprehensive method to identify IGE and SSCI. Section 4 analyzes the characteristics of SSCI and verifies the SSCI-triggered condition. An SSCI-triggered damping control strategy is proposed in Section 5, followed by Section 6, which concludes the article.

2.   SSCI PHENOMENON ANALYSIS

SSCI is the interaction between the RSC controller of a DFIG-based wind turbine and the series-compensated line. It can cause fast undamped SSO of the voltage, current, and power output by the DFIG-based wind turbine generator, as shown in Figure 1 [14]. Recently, similar phenomena have happened in some wind farms of China [23], so the problem is a concern. In the following analysis, the mathematical model including a DFIG-based wind turbine connected to a series-compensated line is built, and the interacting path and the triggered condition of SSCI are analyzed in detail.

The stator equations of a DFIG adopt a generator convention, while the rotor equations of DFIG adopt a motor convention. Under the *dq* rotating coordinate system, the equations of the voltage and flux linkage in the stator and rotor [24] can

FIGURE 1. Oscillography recorded in an SSCI event [14].
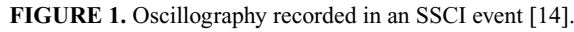
be expressed as

$$\begin{cases} u_{sd} = -R_s i_{sd} - p\psi_{sd} + \omega_s \psi_{sq} \\ u_{sq} = -R_s i_{sq} - p\psi_{sq} - \omega_s \psi_{sd} \end{cases}, \qquad (1)$$

$$\begin{cases} u_{rd} = R_r i_{rd} + p\psi_{rd} - (\omega_s - \omega_r)\psi_{rq} \\ u_{rq} = R_r i_{rq} + p\psi_{rq} + (\omega_s - \omega_r)\psi_{rd} \end{cases}, \qquad (2)$$

$$\begin{cases} \psi_{sd} = L_s i_{sd} - L_m i_{rd} \\ \psi_{sq} = L_s i_{sq} - L_m i_{rq} \end{cases}, \qquad (3)$$

$$\begin{cases} \psi_{rd} = -L_m i_{sd} + L_r i_{rd} \\ \psi_{rq} = -L_m i_{sq} + L_r i_{rq} \end{cases}, \qquad (4)$$

where

p is the differential operator;

u_{sd}, u_{sq}, i_{sd}, and i_{sq} are, respectively, the d and q components of the voltage and current of the stator;

u_{rd}, u_{rq}, i_{rd}, and i_{rq} are, respectively, the d and q components of the voltage and current of the rotor;

ψ_{sd}, ψ_{sq}, ψ_{rd}, and ψ_{rq} are, respectively, the d and q components of the flux linkage in the stator and rotor;

ω_s and ω_r are, respectively, the electrical angle speeds of the stator and the rotor;

R_s and R_r are, respectively, the resistors of the stator and rotor; and

L_s, L_r, and L_m are, respectively, the equivalent self-inductances of the stator and rotor and the mutual inductance.

$L_s = L_{ss} + 1.5L_{mm}$, $L_r = L_{rr} + 1.5L_{mm}$, and $L_m = 1.5L_{mm}$, where L_{ss}, L_{rr}, and L_{mm} are, respectively, the leakage inductances of the stator and rotor and the mutual inductance.

The DFIG adopts a stator flux oriented method by which stator flux ψ_1 is forced to be in phase with the d-axis under the dq rotating coordinate system. Therefore, d- and q-axis stator flux components can be expressed as

$$\begin{cases} \psi_{sd} = \psi_1 \\ \psi_{sq} = 0 \end{cases}. \qquad (5)$$

FIGURE 2. RSC control block diagram of a DFIG.

Assuming the stator flux is constant and the stator resistor is omitted, according to Eq. (1), the d- and q-axis stator voltage components are, respectively,

$$\begin{cases} u_{sd} = 0 \\ u_{sq} = -\omega_s \psi_1 \end{cases}. \qquad (6)$$

With Eqs. (5) and (6) substituted into Eqs. (2)–(4), the d and q incremental components of the voltage and current can be expressed as

$$\begin{cases} \Delta u_{rd} = R_r \Delta i_{rd} - a_2(\omega_s - \omega_r)\Delta i_{rq} + a_2 p \Delta i_{rd} \\ \Delta u_{rq} = R_r \Delta i_{rq} + a_2(\omega_s - \omega_r)\Delta i_{rd} + a_2 p \Delta i_{rq} \end{cases}, \qquad (7)$$

$$\begin{cases} \Delta i_{rd} = -\Delta i_{sd}/a_1 \\ \Delta i_{rq} = -\Delta i_{sq}/a_1 \end{cases}, \qquad (8)$$

where

Δu_{rd} and Δu_{rq} are, respectively, the d and q incremental components of the voltages in the rotor;

Δi_{rd} and Δi_{rq} are, respectively, the d and q incremental components of the currents in the rotor;

Δi_{sd} and Δi_{sq} are, respectively, the d and q incremental components of the currents in the stator; and

ω_s and ω_r are, respectively, the electrical angle speeds of the stator and rotor.

Additionally, $a_1 = -L_m/L_s$ and $a_2 = L_r - L^2_m/L_s$.

Since the SSCI is mainly caused by the interaction between the RSC of the DFIG and the power grid, the RSC control of the DFIG shown in Figure 2 is considered to analyze SSCI, and the dq decoupling closed-loop control is adopted [21, 25]. In Figure 2, the constant reactive power control is used in the d-axis, while the active power acquired from the maximum wind tracking is provided as the reference value of the control in the q-axis to regulate the active power output by the DFIG.

According to Eq. (7) and the control strategy shown in Figure 2, the rotor incremental current equations in the d- and
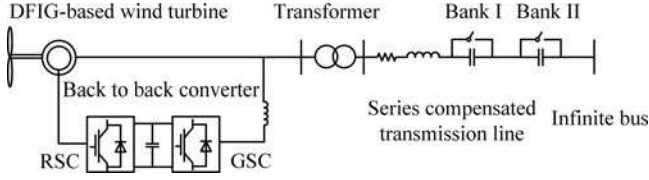
FIGURE 3. Structure diagram of test system.

q-axes are

$$\begin{cases} a_2 p\Delta i_{rd} = [-\Delta q_s(k_{g1}+k_{i1}/p)/a_1 - \Delta i_{rd}](k_{g2}+k_{i2}/p) \\ a_2 p\Delta i_{rq} = [-\Delta p_s(k_{g1}+k_{i1}/p)/a_1 - \Delta i_{rq}](k_{g2}+k_{i2}/p) \end{cases}, \quad (9)$$

where Δq_s and Δp_s are, respectively, the incremental reactive and active powers output by the DFIG; k_{g1}, k_{i1}, k_{g2}, and k_{i2} are, respectively, the outer and inner loop gains of the RSC controller.

The system structure diagram including a single DFIG-based wind turbine connected to a fixed series-compensated transmission line is shown in Figure 3.

Assuming the voltage at the terminal of the DFIG in Figure 3 is perfect sine, the a phase voltage can be expressed as

$$u_{sa} = \sqrt{2}U_s \sin(\omega_s t + \phi_{us}), \quad (10)$$

where U_s and φ_{us} are, respectively, the RMS value and the initial phase of the fundamental voltage.

When there are three-phase symmetrical resonance currents at the subsynchronous frequency ω_n existing in the fixed series-compensated transmission line caused by the system disturbance, without considering the harmonic influence, the a phase current output by the DFIG can be expressed as

$$i_{sa} = \sqrt{2}I_s \sin(\omega_s t + \phi_{is}) + \sqrt{2}I_n \sin(\omega_n t + \phi_{in}), \quad (11)$$

where I_s and φ_{is} are, respectively, the RMS value and initial phase of the fundamental current; I_n, ω_n, and φ_{in} are, respectively, the RMS value, angular frequency, and initial phase of the a phase subsynchronous current.

According to the constant power transformation matrix **C** from abc to dq as shown in Eq. (12), the voltages and currents in the d- and q-axes can be expressed as Eqs. (13) and (14):

$$\mathbf{C} = \sqrt{\frac{2}{3}}$$

$$\times \begin{bmatrix} \cos(\omega_s t + \phi_{us}) & \cos(\omega_s t + \phi_{us} - \frac{2\pi}{3}) & \\ & & \cos(\omega_s t + \phi_{us} + \frac{2\pi}{3}) \\ -\sin(\omega_s t + \phi_{us}) & -\sin(\omega_s t + \phi_{us} - \frac{2\pi}{3}) & \\ & & -\sin(\omega_s t + \phi_{us} + \frac{2\pi}{3}) \\ \frac{1}{2} & \frac{1}{2} & \frac{1}{2} \end{bmatrix}, \quad (12)$$

$$\begin{cases} u_{sd} = 0 \\ u_{sq} = -\sqrt{3}U_s \end{cases}, \quad (13)$$

$$\begin{cases} i_{sd} = -\sqrt{3}I_s \sin(\phi_{us} - \phi_{is}) - \sqrt{3}I_n \sin((\omega_s - \omega_n)t + \phi_i) \\ \qquad = i_{sd0} + i_{sd\_sub} \\ i_{sq} = -\sqrt{3}I_s \cos(\phi_{us} - \phi_{is}) - \sqrt{3}I_n \cos((\omega_s - \omega_n)t + \phi_i) \\ \qquad = i_{sq0} + i_{sq\_sub} \end{cases}, \quad (14)$$

where φ_i is the difference between φ_{us} and φ_{in}; i_{sd0} and i_{sq0} are, respectively, the DC components of the stator currents in the d- and q-axes; and i_{sd_sub} and i_{sq_sub} are, respectively, the subsynchronous components of the stator currents in the d- and q-axes at the frequency $\omega_s - \omega_n$. Due to the assumption of symmetry, there is no supsynchronous current in the d- and q-axes.

Assuming the controller can track the fundamental active and reactive powers perfectly, in the dq frame, the incremental active and reactive powers output by the DFIG can be calculated as

$$\begin{cases} \Delta p_s = 3U_s I_n \cos[(\omega_s - \omega_n)t + \phi_i] = -\sqrt{3}U_s i_{sq\_sub} \\ \Delta q_s = 3U_s I_n \sin[(\omega_s - \omega_n)t + \phi_i] = -\sqrt{3}U_s i_{sd\_sub} \end{cases}. \quad (15)$$

On one hand, the active and reactive power fluctuations in Eq. (9) can be excited at the frequency $\omega_s - \omega_n$ by the three-phase subsynchronous currents at the frequency ω_n. δq_s and δp_s are, respectively, used as the RSC controller inputs in the d- and q-axes, passing through the proportional and integral regulators in the inner loop and forming the reference values of the rotor currents in the d- and q-axes.

On the other hand, the rotating magnetic field induced by the three-phase subsynchronous currents of the stator cuts the rotor windings of the DFIG. As a result, the three-phase subsynchronous currents at frequency $\omega_r - \omega_n$ are induced in the rotor windings, which have frequency $\omega_s - \omega_n$ seen from the dq frame. According to Eqs. (2) and (8), the d and q incremental components in the rotor currents can be expressed as

$$\begin{cases} \Delta i_{rd} = i_{rd\_sub} = -i_{sd\_sub}/a_1 \\ \Delta i_{rq} = i_{rq\_sub} = -i_{sq\_sub}/a_1 \end{cases}. \quad (16)$$

Actually, Eq. (7) could also describe the transfer path of the subsynchronous components in the RSC control shown in Figure 2 by substituting Eqs. (9), (15), and (16) into Eq. (1). Then the d and q subsynchronous voltage components caused by the RSC controller could be obtained as

$$\begin{cases} \Delta u_{rd} = R_r i_{rd\_sub} - a_2(\omega_s - \omega_r)i_{rq\_sub} - K i_{rd\_sub} \\ \Delta u_{rq} = R_r i_{rq\_sub} + a_2(\omega_s - \omega_r)i_{rd\_sub} - K i_{rq\_sub} \end{cases}, \quad (17)$$

where

$$K = \left[\sqrt{3}U_s(k_{g1}+\frac{k_{i1}}{p})+1\right]\left(k_{g2}+\frac{k_{i2}}{p}\right) = K_1 + \frac{K_2}{p} + \frac{K_3}{p^2} \quad (18)$$

and

$$\begin{cases} K_1 = \sqrt{3}U_s k_{g1} k_{g2} + k_{g2} \\ K_2 = \sqrt{3}U_s(k_{g1}k_{i2} + k_{i1}k_{g2}) + k_{i2} \\ K_3 = \sqrt{3}U_s k_{i1} k_{i2} \end{cases}. \quad (19)$$

The subsynchronous voltages at frequency $\omega_s - \omega_n$ shown in Eq. (17) are then imposed on the rotor windings, and new subsynchronous currents are produced. Equation (17) is substituted into Eq. (7), and the first-order linear differential equations are solved, as shown in Eq. (20):

$$\begin{cases} R_r \Delta i_{rd} - a_2(\omega_s - \omega_r)\Delta i_{rq} + a_2 p \Delta i_{rd} \\ \quad = \frac{\sqrt{3}I_n}{a_1}[R_r \sin((\omega_s - \omega_n)t + \phi_i) - a_2(\omega_s - \omega_r) \\ \quad \cos((\omega_s - \omega_n)t + \phi_i) \\ \quad -(K_1 + \frac{K_2}{p} + \frac{K_3}{p^2})\sin((\omega_s - \omega_n)t + \phi_i)] \\ R_r \Delta i_{rq} + a_2(\omega_s - \omega_r)\Delta i_{rd} + a_2 p \Delta i_{rq} = \\ \quad \frac{\sqrt{3}I_n}{a_1}[R_r \cos((\omega_s - \omega_n)t + \phi_i) + a_2(\omega_s - \omega_r) \\ \quad \sin((\omega_s - \omega_n)t + \phi_i) \\ \quad -(K_1 + \frac{K_2}{p} + \frac{K_3}{p^2})\cos((\omega_s - \omega_n)t + \phi_i)] \end{cases}. \quad (20)$$

Then the solution of the first-order linear differential equations is

$$\begin{cases} \Delta i_{rd} = -\sqrt{3}\frac{|h|I_n}{a_1}\sin((\omega_s - \omega_n)t + \phi_i + \phi) \\ \Delta i_{rq} = -\sqrt{3}\frac{|h|I_n}{a_1}\cos((\omega_s - \omega_n)t + \phi_i + \phi) \end{cases}, \quad (21)$$

where φ and $|h|$ are, respectively, the phase deviation and the amplified amplitude compared with the original resonance current in Eq. (11). φ and $|h|$ can be calculated by Eqs. (22) and (23):

$$\phi = \tan^{-1}\frac{R_r\omega_1[K_2 - a_2\omega_1^2] - a_2\omega_2[K_3 - \omega_1^2 K_1]}{a_2\omega_1\omega_2[K_2 - a_2\omega_1\omega_3] + R_r[\omega_1^2(R_r - K_1) + K_3]}, \quad (22)$$

$$|h| = \left|\frac{(R_r - K_1)\omega_1^2 + K_3}{\omega_1^2[R_r\cos\phi - a_2\omega_2\sin\phi]}\right|, \quad (23)$$

where ω_1, ω_2, and ω_3 follow Eq. (24):

$$\begin{cases} \omega_1 = \omega_s - \omega_n \\ \omega_2 = \omega_r - \omega_n \\ \omega_3 = \omega_s - \omega_r \end{cases}. \quad (24)$$

According to Eq. (16), the subsynchronous currents in the rotor windings in Eq. (21) caused by the RSC controller further induces the subsynchronous currents in the stator windings as

$$\begin{cases} \Delta i_{sd} = \sqrt{3}|h|I_n\sin((\omega_s - \omega_n)t + \phi_i + \phi) \\ \Delta i_{sq} = \sqrt{3}|h|I_n\cos((\omega_s - \omega_n)t + \phi_i + \phi) \end{cases}. \quad (25)$$

Transforming the currents in Eq. (25) into the *abc* reference frame, the *a* phase subsynchronous current induced in the stator winding is

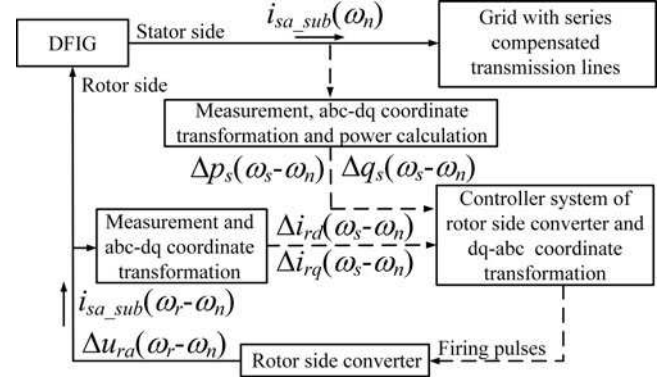$$\Delta i_{sa\_sub} = \sqrt{2}|h|I_n\sin(\omega_n t + \phi_{in} - \phi + \pi). \quad (26)$$
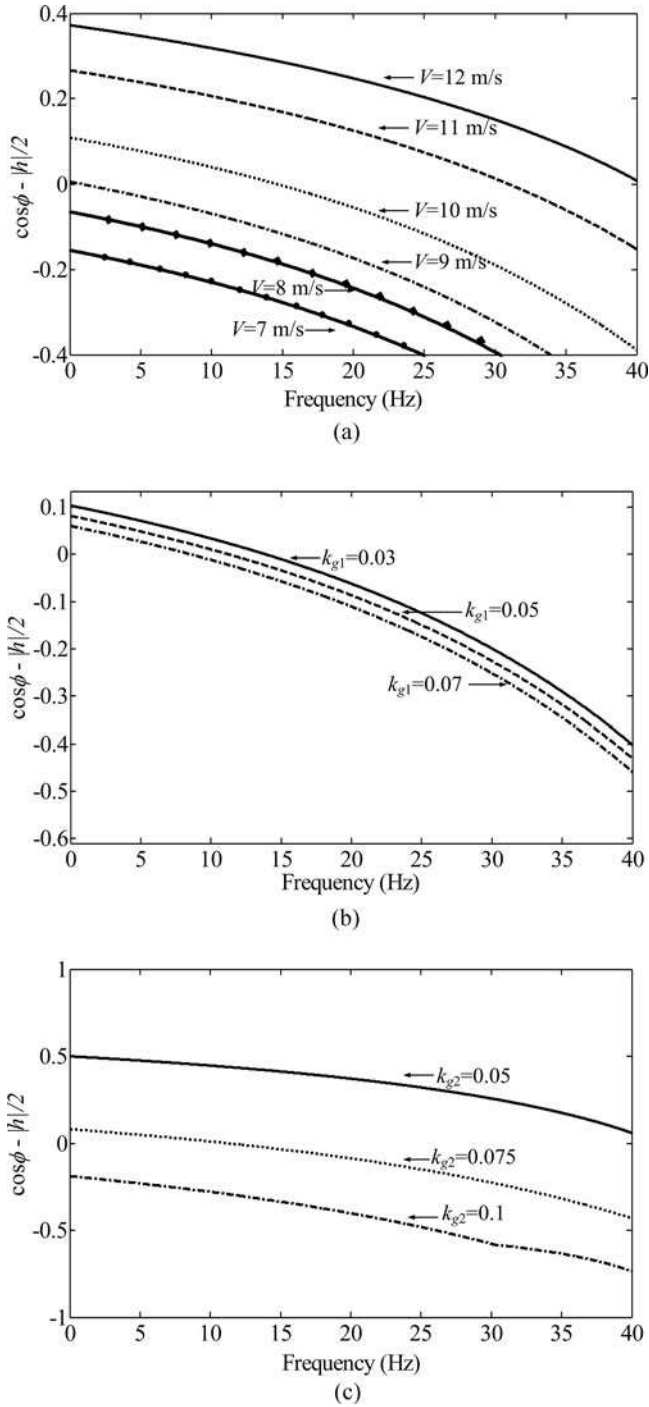

FIGURE 4. SSCI block diagram.

If the current in Eq. (26) increases the original resonance current containing the current in Eq. (11), the disturbance will be further amplified and the subsynchronous current at frequency ω_n will be gradually increased due to the positive feedback. Subsequently, the mutual excitation will be formed between the RSC controller of the DFIG and the series-compensated transmission line, which can lead to fast-growing oscillations of the active and reactive powers output by the DFIG-based wind turbine. According to the analysis above, the condition that triggers the fast growing oscillation can be expressed as

$$Mag\left\{\sqrt{2}|h|I_n\sin(\omega_n t + \phi_{in} - \phi + \pi) + \sqrt{2}I_n\sin(\omega_n t + \phi_{in})\right\} > Mag\left\{\sqrt{2}I_n\sin(\omega_n t + \phi_{in})\right\} = \sqrt{2}I_n. \quad (27)$$

Then the following can be obtained:

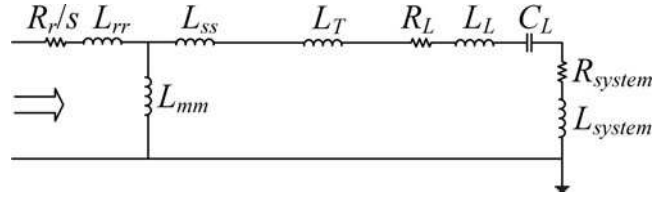$$\cos\phi < \frac{|h|}{2}. \quad (28)$$

Hence, the SSCI can be illustrated using the diagram shown in Figure 4. When there is subsynchronous current in the series-compensated transmission line due to the disturbance, the RSC controller will be influenced due to the introduced active and reactive power controls. On the other hand, the subsynchronous current can also affect the inner loop of the RSC controller by inducing the subsynchronous current into the rotor. As a result, the RSC controller feeds back its influence to the DFIG and the grid; it then increases the subsynchronous current in the transmission line if the condition in Eq. (27) or (28) is satisfied. Figure 5 shows different curves of the variable $\cos\varphi - |h|/2$ as a function of the resonance frequency with different wind speeds and different inner and outer loop gains. It can be seen from Figure 5 that the system is vulnerable to SSCI with larger resonanace frequency, *i.e.*, higher compensation level, lower wind speed, and larger inner and outer loop gains.

FIGURE 5. Different curves of the variable $\cos\varphi - |h|/2$ as a function of the resonance frequency: (a) different wind speeds, (b) different outer loop gains, and (c) different inner loop gains.

FIGURE 6. Equivalent circuit used for IGE analysis.

frequency of the shaft. However, according to the analysis presented in Section 2, SSCI happens among the DFIG, the RSC and its controller, and the series-compensated transmission lines. While the IGE is just the interaction between the DFIG and series-compensated transmission lines. This concludes that the path of the IGE is contained in the path of the SSCI, as shown in Figure 3. Hence, an effective method should be proposed to identify the real reason of non-torsional SSO and proper mitigation methods adopted separately. Impedance scanning and the SSCI-triggered condition are combined to separate the two non-torsional SSO phenomena in this section. Furthermore, the shaft model with a single cylinder for excluding TI is used to do the time-domain simulation to verify the proposed method.

3.1. IGE identification

The equivalent circuit of the induction generator shown in Figure 6 is used to identify IGE by impedance scanning. In Figure 6, L_T denotes the leakage inductance of the transformer; R_L, L_L, and C_L are, respectively, the resistance, inductance and capacitance of the series-compensated transmission line; R_{system} and L_{system} are, respectively, the equivalent resistance and inductance of the system. If the equivalent resistance is negative at the point where the equivalent reactance approaches to zero, according to the principle of IGE, it will appear in this system.

The parameters of the induction generator are shown in Table 1, where the impedance of the induction generator is normalized by the rated power and voltage of the DFIG. With a 40% series compensation level, the equivalent reactance and equivalent resistance varying with the frequency are shown in Figure 7, respectively, under the ratios of the reactance to resistance 1.5 and 3.0. When the ratio of the reactance to resistance is 1.5, the equivalent resistance is positive at the resonance frequency of 11 Hz, meaning there is no risk of IGE. When the ratio of the reactance to resistance is increased to 3.0, the equivalent resistance shows negative at the resonance frequency, meaning that there is a risk of IGE.

Time-domain simulation is used to further verify the conclusion above. To exclude the SSCI, the RSC and GSC controllers are both blocked, and the three-phase rotor windings are shorted. Now the DFIG is equivalent to a general induc-

3. IDENTIFICATION FOR IGE AND SSCI

IGE and SSCI can be both classified into a non-torsional SSO, which is irrelevant to the shaft of the DFIG. TI, which rarely happens for DFIG-based wind turbines, can be easily identified due to its frequency correlation with the natural

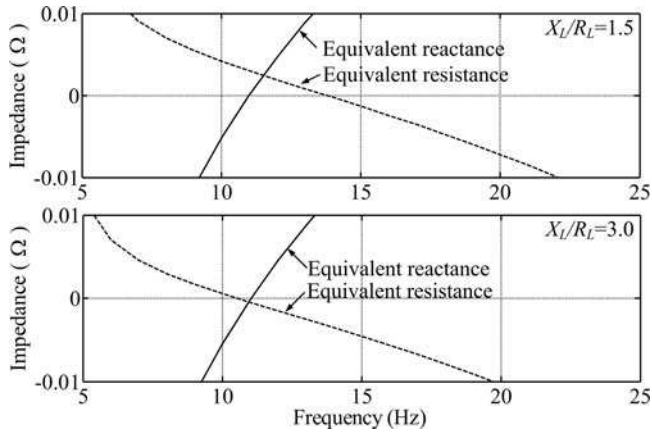| Parameter	Value
Rated power	1.5 MW
Rated voltage	0.69 kV
Grid frequency	50 Hz
Leakage reactance of the stator	0.177 p.u.
Resistance of the rotor	0.1 p.u.
Leakage reactance of the rotor	0.116 p.u.
Excitation reactance	4.68 p.u.

TABLE 1. Parameters of the Induction generator.

Parameter	Value
Rated power	1.5 MW
Blade length	35 m
Maximum performance coefficient	0.44
Air density	1.225 kg/m^3

TABLE 2. Parameters of the wind turbine.

Parameter	Value
k_{g1}	0.05
k_{i1}	1.0
k_{g2}	0.075
k_{i2}	1.0

TABLE 3. PI parameters of the RSC controller.

FIGURE 7. Impedance-frequency characteristic of the system at subsynchronous frequencies.

tion generator. When series-compensated capacitor bank I is switched on, with the same ratios of the reactance to resistance as mentioned above, the active and reactive power oscillations as shown in Figure 8(a) indicate a consistent conclusion with the above analysis. Therefore, IGE can be identified.

3.2.   SSCI identification

The SSCI can be identified based on the analysis proposed in Section 2. According to the parameters of the induction generator shown in Table 1, the parameters of the wind turbine shown in Table 2, and the PI parameters of the RSC controller shown in Table 3, the SSCI-triggered condition can be calculated as follows using Eqs. (22) and (23):

$$\begin{cases} \cos \phi = 0.2236 \\ |h|\,/2 = 0.2767 \end{cases}. \tag{29}$$

According to Eq. (28), Eq. (29) indicates that there is a risk of SSCI under the two different ratios of the reactance to resistance, which is further verified using time-domain simulation. Considering the RSC and GSC controllers, when series-compensated capacitor bank I is switched on, the active and reactive power oscillations are shown in Figure 8(b).
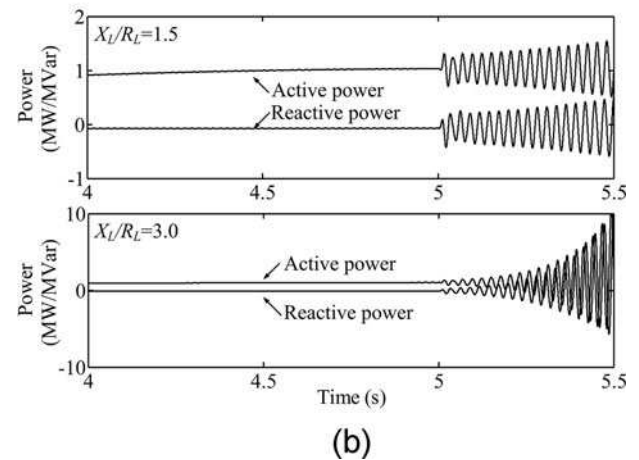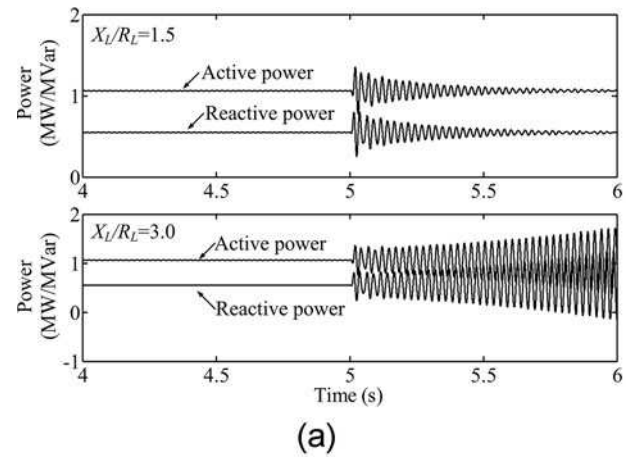

FIGURE 8. Active and reactive power with different ratios of reactance to resistance: (a) analysis for IGE and (b) analysis for both IGE and SSCI.

When the ratio of the reactance to resistance is 1.5, in which condition there is no IGE, the fast-growing oscillations of the active and reactive powers shown in Figure 8(b) conclude the existence of SSCI. If the ratio of the reactance to resistance is increased to 3.0, in which condition IGE exists as shown in Figure 8(a), the active and reactive powers have significant fast-growing oscillations over that in Figure 8(a), indicating that IGE and SSCI are determined to coexist. Therefore, SSCI can be identified effectively, regardless of whether IGE exists.

4.   CHARACTERISTIC ANALYSIS OF SSCI

As it can be seen from Eqs. (22), (23), and (28), the existence of SSCI mainly depends on the rotating speed of the DFIG, which can also reflect wind speed V, the disturbance frequency (*i.e.*, the series compensation level k), and the RSC controller parameters, especially the controller gains. The system in Figure 3 is used to further verify Eq. (28) by time-domain simulation.

It can be seen from Figures 9(a) and 9(b) that the effect of SSCI is gradually reduced as the wind speed increases. And as the series compensation level in the transmission line increases, shown in Figures 10(a) and 10(b), the effect of SSCI is gradually increased. Moreover, as seen from Figures 11(a), 11(b), 11(c), and 11(d), the increase of the outer or inner gain in the RSC controller may also lead to SSCI. Compared with the outer gain, the seriousness of SSCI is more sensitive to the change of the inner gain. Additionally, the occurrence of SSCI in the time-domain simulation shown in Figures 8–10 is totally consistent with the SSCI-triggered condition in Eq. (28) and Figure 5.

## 5.   SSCI-TRIGGERED DAMPING CONTROL STRATEGY

According to the characteristics analysis presented in Section 4, the inner and outer gains in the RSC controller could be properly reduced in the allowed ranges to mitigate SSCI. However, this kind of method is limited, so a supplementary damping control strategy should be proposed.

Based on the analysis in Section 2 and the simulation verification in Section 4, the SSCI-triggered condition in Eq. (28) can be accurately used to decide whether SSCI has happened in the system. Therefore, the condition can also be adopted to start a damping control in the RSC controller. This way, the influence of damping control on the controller can be reduced to the minimum in a normal operating condition when no SSCI exists. On the other hand, the damping control will not frequently take up the capacity of the DFIG when there is no risk of SSCI.

The RSC control diagram with the SSCI-triggered damping control strategy is shown in Figure 12. The RSC control consists of four parts: the SSCI frequency acquisition, the SSCI judgment, the damping control, and the dq decoupling control.

Since the frequency of SSCI varies with the structure or operating condition of the power grid, a method based on a single SSCI frequency is used in this study to acquire the oscillation frequency. When there is only one oscillation frequency ω_n in the transmission line current, as shown in Eq. (11), the active and reactive powers could be used to acquire the oscillation frequency more easily. As shown in Figure 12, the high-pass filters are used to remove the DC component in the active power, which corresponds to the fundamental component in the three-phase currents. The amplitude-frequency and phase-frequency characteristics of the high-pass filter are shown in Figure 13. Then oscillation component δp_s in the active power with frequency $\omega_s - \omega_n$ shown in Eq. (15) remains, and ω_n can be further calculated by the division between the derivative of δp_s and itself as shown in Figure 12.

ω_n and the rotating speed of DFIG ω_r are both required to calculate $\cos\varphi$ and $|h|/2$ based on Eqs. (22) and (23), and the status of the damping control can then be determined according to the condition shown in Eq. (28). A hysteresis module is adopted in the control strategy shown in Figure 12 with two input thresholds: $\gamma_{\min}$ and $\gamma_{\max}$. The input threshold $\gamma_{\min}$ is properly chosen as a margin considering the parameter uncertainties, so $\gamma_{\min}$ must be positive. The hysteresis region, *i.e.*, $\gamma_{\max} - \gamma_{\min}$, is properly chosen to avoid a continuous switching condition. The values of $\gamma_{\min}$ and $\gamma_{\max}$ are shown in Table 4. When the condition is satisfied, the damping control is inserted into the RSC controller by setting K to 1. The damping control acquires oscillation components of the active and reactive powers of the wind turbine by the band-pass filters. The parameters of the damping control are shown in Table 4. Since the frequency of the SSCI must be measured on-line, not every resonance frequency could get the optimal damping effect. Therefore, fourth-order Butterworth filters with a wide band are adopted in this control strategy. The upper and lower cutoff frequencies of the band-pass filters are designed according to the frequency $\omega_s - \omega_n$ in the range of subsynchronous frequency shown in Table 4. Furthermore, the amplitude-frequency and phase-frequency characteristics shown in Figure 14 are designed to keep the phase variation and amplified gain as small as possible in the range of the subsynchronous frequency. Also, to further enhance the damping effect, the gains of the damping control in the d- and q-axes are properly increased without influencing the normal function of the RSC controller, which are shown in Table 4. Each of the oscillation components is used as one of the inner loop inputs in the d- and q-axes, which involve the feedback control for
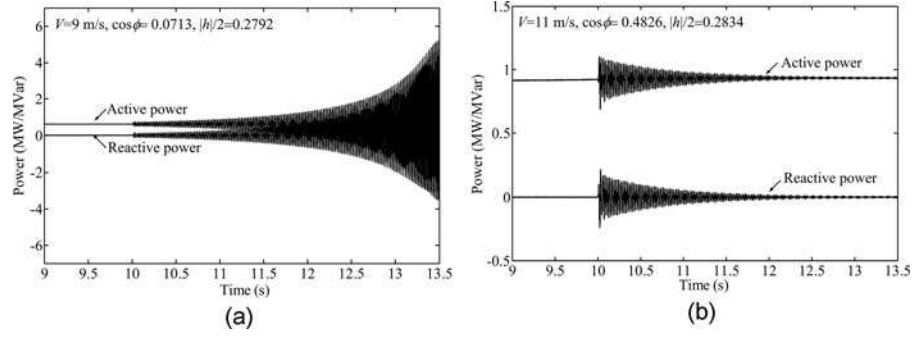
FIGURE 9. Active and reactive power with different wind speed V: (a) $V = 9$ m/s with $\cos\varphi = 0.0713$ and $|h|/2 = 0.2792$ and (b) $V = 11$ m/s with $\cos\varphi = 0.4826$ and $|h|/2 = 0.2834$.
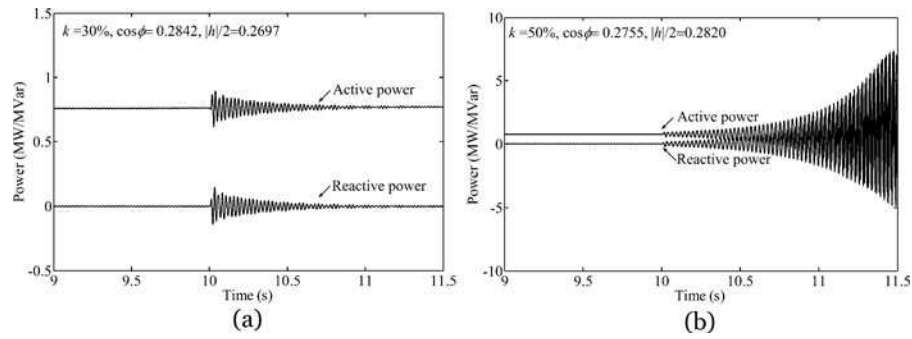
FIGURE 10. Active and reactive power with different series compensation level k: (a) $k = 30\%$ with $\cos\varphi = 0.2842$ and $|h|/2 = 0.2697$ and (b) $k = 50\%$ with $\cos\varphi = 0.2755$ and $|h|/2 = 0.2820$.
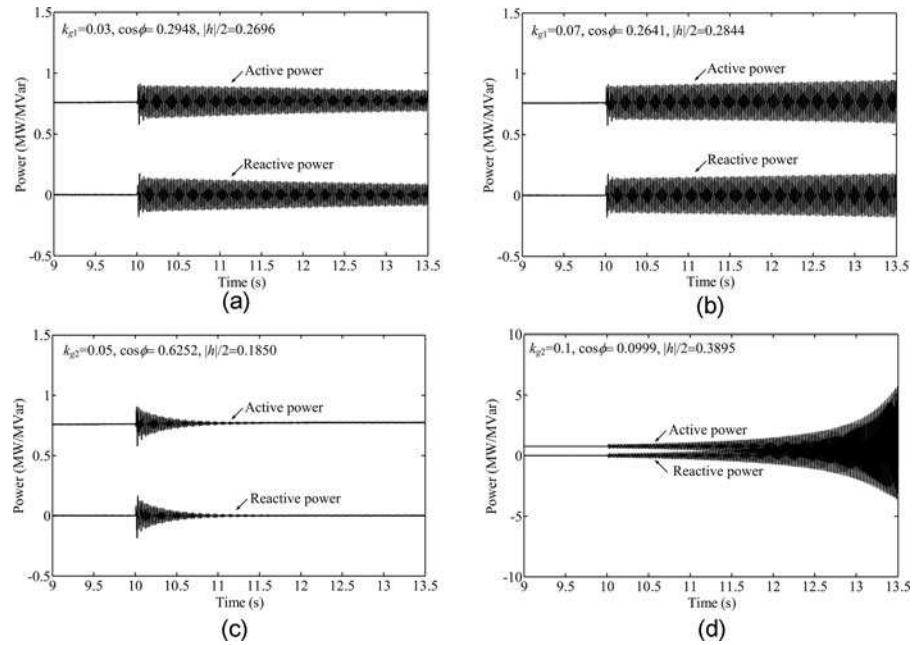
FIGURE 11. Active and reactive power with different outer and inner gains of the RSC controller: (a) $k_{g1} = 0.03$ with $\cos\varphi = 0.2948$ and $|h|/2 = 0.2696$, (b) $k_{g1} = 0.07$ with $\cos\varphi = 0.2641$ and $|h|/2 = 0.2844$, (c) $k_{g2} = 0.05$ with $\cos\varphi = 0.6252$ and $|h|/2 = 0.1850$, and (d) $k_{g2} = 0.1$ with $\cos\varphi = 0.0999$ and $|h|/2 = 0.3895$.
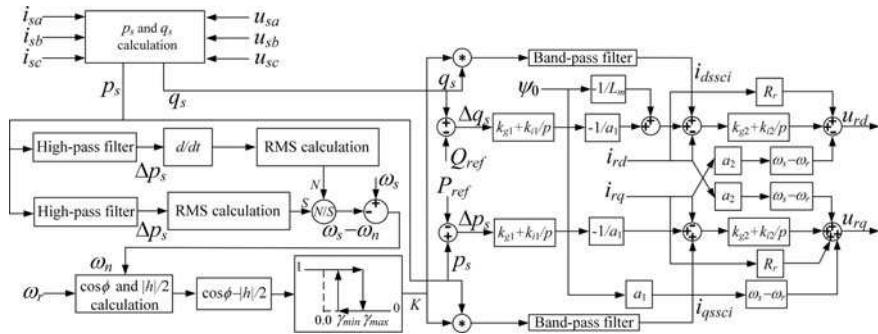
FIGURE 12. RSC control block diagram with the SSCI-triggered damping control.
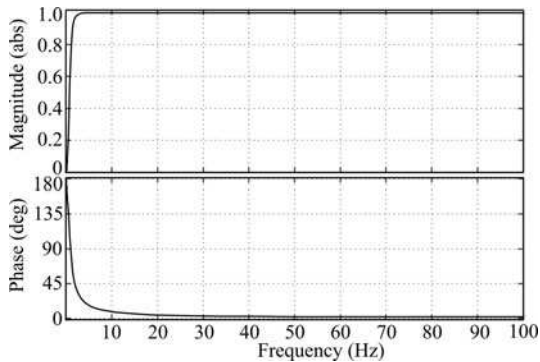

FIGURE 13. Amplitude-frequency and phase-frequency characteristics of the high-pass filter.
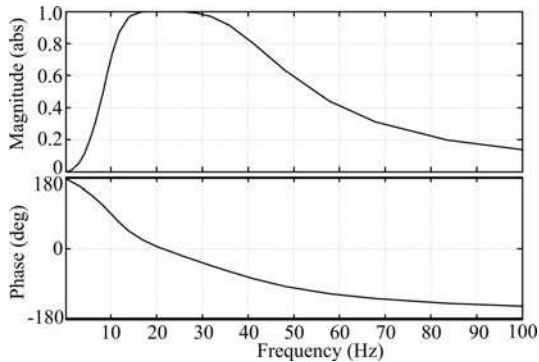

FIGURE 14. Amplitude-frequency and phase-frequency characteristics of the band-pass filter.

damping SSCI. When the condition is not satisfied, the damping control is blocked by setting K to 0 and the RSC controller works in normal operating condition (*i.e.*, the constant reactive power control and the maximum wind tracking control).

The simulation system shown in Figure 3 is used to verify the effectiveness of the above-mentioned SSCI-triggered damping control. Assuming IGE and TI problems are better resolved, the ratio of the reactance to resistance is set to 3.0, and the shaft model with a single cylinder is adopted in the simulation. The parameters in Tables 1–4 are adopted in the following simulation.

|		
	$\gamma_{\min}$	0.05
Hysteresis	$\gamma_{\max}$	0.07
Band-pass filter	Type	Fourth-order Butterworth
	Upper cutoff frequency	45 Hz
	Lower cutoff frequency	10 Hz
	d-axis gain	3
	q-axis gain	4

TABLE 4. Parameters of the SSCI-triggered damping controller

Figure 15(a) shows the oscillations of the active and reactive powers output by the wind turbine and the change of the SSCI-triggered condition following the change of the wind speed before the mitigation measure is taken. When the wind speed is 11 m/s, $\cos\varphi$ is bigger than $|h|/2$, meaning no SSCI will happen. So at time 10 sec, when series-compensated capacitor bank I is switched on the transmission lines, the oscillations of the active and reactive powers are convergent. Hence, with the decrease of the wind speed, the active power output by the DFIG decreases and $\cos\varphi$ decreases. When $\cos\varphi$ goes across $|h|/2$, meaning the SSCI-triggered condition is satisfied, the oscillations of the active and reactive powers begin to grow and diverge gradually.

Figure 15(b) shows the power oscillations output by the wind turbine and the change of the SSCI-triggered condition following the change of the wind speed after the mitigation measure is taken. When $\cos\varphi - |h|/2$ is equal to $\gamma_{\min}$, K is switched to 1, the damping control is enabled, and the power oscillations are damped successfully. When the wind speed stays at 9 m/s, a condition at which the system is vulnerable to SSCI, the damping control remains able to stabilize the system. As the wind speed increases, $\cos\varphi$ goes across $|h|/2$ again, meaning the SSCI-triggered condition is not satisfied. When
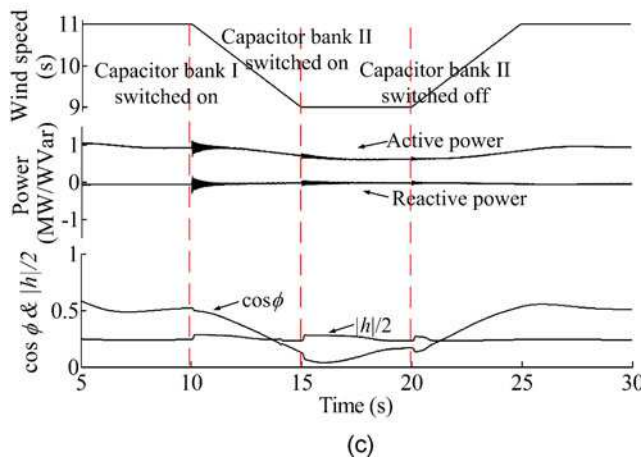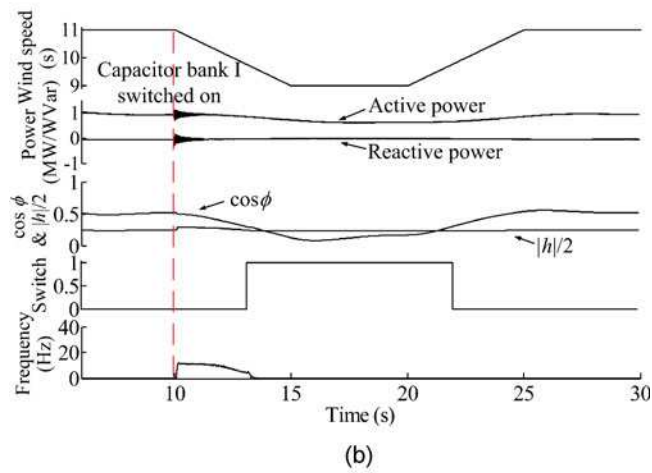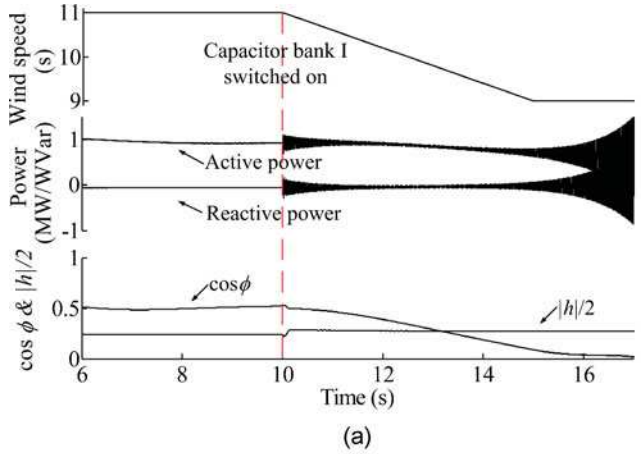
FIGURE 15. Simulation results with the change of the wind speed and capacitor bank I switched: (a) without SSCI-triggered damping control, (b) with SSCI-triggered damping control following capacitor bank I switched, and (c) with SSCI-triggered damping control following capacitor bank I and II switched.
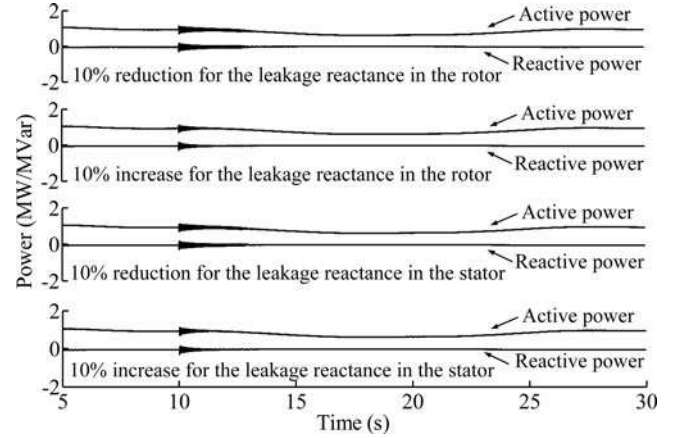

FIGURE 16. Simulation results with the change of the reactance in the rotor and stator.

$\cos\varphi$-$|h|/2$ is equal to γ_{max}, the damping control is blocked and the system is still stable.

Figure 15(c) shows the power oscillations output by the DFIG and the SSCI-triggered condition with the change of the wind speed as well as capacitor banks I and II switched when the SSCI-triggered damping control strategy is adopted. Similar to the scenario above, capacitor bank I is switched on from time 10 sec. At time 15 sec, when capacitor bank II is switched on, the power oscillations with the series compensation level increased, and lower wind speed can still converge quickly since the damping control remains enabled in the controller, indicating the effectiveness of the proposed control strategy.

To analyze effects of the parameter uncertainty and verify the robustness of the proposed method, a 10% increase and reduction of the original values of the leakage reactance in the stator and the rotor are, respectively, used in the simulation. It can been seen from the simulation result in Figure 16 that the changes in the leakage reactance have small effect on the triggering of the SSCI damping control, and the damping ability is still very strong.

The method proposed in [18] is used to compare with the proposed method herein, which respectively, added low-pass filters to the P_s, i_{rd}, and i_{rq} measurement signals in the RSC controller. It can be seen from Figure 17(a) that the method of adding low-pass filters could mitigate SSCI with a 40% compensation level. As the compensation level increases to 60%, as shown in Figure 17(b), however, the method could not mitigate SSCI effectively compared with the proposed method, which has better mitigation ability. In addition, since the damping control is active only if SSCI happens, the method proposed herein does not influence the work of the RSC controller in normal conditions compared with other damping control methods.
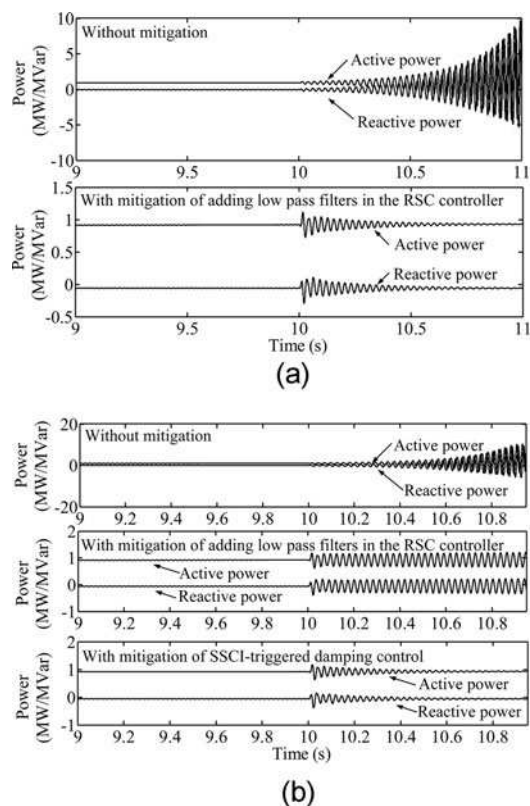
FIGURE 17. Simulation results with different compensation levels using different methods: (a) with 40% compensation level and (b) with 60% compensation level.

6. CONCLUSION

This article elaborates on SSCI phenomenon that occurs between the RSC controller of a DFIG-based wind turbine and a fixed series-compensated transmission line. According to the analysis, if the original disturbance current is amplified due to the mutual excitation, SSCI will happen. An SSCI-triggered condition is proposed by the SSCI analysis. And a method combining the SSCI-triggered condition with impedance scanning is presented to identify IGE and SSCI, which have a similar interaction path. Time-domain simulation indicates that the decrease of the wind speed, the increase of the series compensation level, and the RSC controller gains can increase the risk of SSCI. Furthermore, time-domain simulation also indicates that the SSCI-triggered condition can exactly identify the SSCI problem with the changes of the wind speed, series compensation level, and RSC controller gains. Also, a damping control strategy based on the SSCI-triggered condition is proposed and designed to mitigate SSCI. The simulation results demonstrate that the SSCI-triggered damping control could effectively mitigate SSCI even under the condition of parameter variation. Compared with other methods, the damping control proposed in this article could effectively mitigate SSCI at higher series compensation level.

REFERENCES

[1] Song, J., Krishnamurthy, V., Kwasinski, A., and Sharma, R., "Development of a Markov-chain-based energy storage model for power supply availability assessment of photovoltaic generation plants," *IEEE Trans. Sustain. Energy*, Vol. 4, No. 2, pp. 491–500, April 2013.

[2] Haque, A. U., Nehrir, M. H., and Mandal, P., "A hybrid intelligent model for deterministic and quantile regression approach for probabilistic wind power forecasting," *IEEE Trans. Power Systems*, Vol. 29, No. 4, pp. 1663–1672, July 2014.

[3] Rahman, M. L., Oka, S., and Shirai, Y., "Hybrid power generation system using offshore-wind turbine and tidal turbine for power fluctuation compensation (HOT-PC)," *IEEE Trans. Sustain. Energy*, Vol. 1, No. 2, pp. 92–98, July 2010.

[4] Mei, S., Zhang, D., Wang, Y., Liu, F., and Wei, W., "Robust optimization of static reserve planning with large-scale integration of wind power: A game theoretic approach," *IEEE Trans. Sustain. Energy*, Vol. 5, No. 2, pp. 535–545, April 2014.

[5] Nayak, P. K., Pradhan, A. K., and Bajpai, P., "Wide-area measurement-based backup protection for power network with series compensation," *IEEE Trans. Power Del.*, Vol. 29, No. 4, pp. 1970–1977, August 2014.

[6] Wang, L., Xie, X., Jiang, Q., and Pota, H. R., "Mitigation of multimodal subsynchronous resonance via controlled injection of supersynchronous and subsynchronous currents," *IEEE Trans. Power Syst.*, Vol. 29, No. 3, pp. 1335–1344, May 2014.

[7] Adrees, A., and Milanovic, J. V., "Methodology for evaluation of risk of subsynchronous resonance in meshed compensated networks," *IEEE Trans. Power Syst.*, Vol. 29, No. 2, pp. 815–823, March 2014.

[8] Varma, R. K., Auddy, S., and Semsedini, Y., "Mitigation of subsynchronous resonance in a series-compensated wind farm using FACTS controllers," *IEEE Trans. Power Del.*, Vol. 23, No. 3, pp. 1645–1654, July 2008.

[9] Zhu, C., Hu, M., and Wu, Z., "Parameters impact on the performance of a double-fed induction generator-based wind turbine for subsynchronous resonance control," *IET Renew. Power Gener.*, Vol. 6, No. 2, pp. 92–98, March 2012.

[10] Alawasa, K. M., Mohamed, Y. A.-R. I, and Xu, W., "Modeling, analysis, and suppression of the impact of full-scale wind-power converters on subsynchronous damping," *IEEE Syst. J.*, Vol. 7, No. 4, pp. 700–712, December 2013.

[11] Leon, A. E., Mauricio, J. M., and Solsona, J. A., "Subsynchronous resonance mitigation using variablespeed wind energy conversion systems," *IET Gener. Transm. Distrib.*, Vol. 7, No. 5, pp. 511–525, May 2013.

[12] Fan, L., Kavasseri, R., Miao, Z. L., and Zhu, C., "Modeling of DFIG-based wind farms for SSR analysis," *IEEE Trans. Power Del.*, Vol. 25, No. 4, pp. 2073–2082, October 2010.

[13] Badrzadeh, B., and Saylors, S., "Susceptibility of wind turbines to sub-synchronous control and torsional interaction," *2012 IEEE PES Transmission and Distribution Conference and Exposition (T&D)*, Paper no. 12963607, pp. 1–8, Orlando, FL, 7–10 May 2012.

[14] Gross, Jr., L. C., "Sub-synchronous grid conditions: New event, new problem, and new solutions," *Western Protective Relay Conference*, Spokane, WA, 19–21 October 2010.

[15] Adams, J., Carter, C., and Huang, S.-H., "ERCOT experience with sub-synchronous control interaction and proposed remediation," *2012 IEEE PES Transmission and Distribution Conference and Exposition (T&D)*, Paper no. 12963672, pp. 1–5, Orlando, FL, 7–10 May 2012.

[16] Nath, R., and Grande-Moran, C., "Study of sub-synchronous control interaction due to the interconnection of wind farms to a series compensated transmission system," *2012 IEEE PES Transmission and Distribution Conference and Exposition (T&D)*, Paper no. 12963609, pp. 1–6, Orlando, FL, 7–10 May 2012.

[17] Suriyaarachchi, D. H. R., Annakkage, U. D., Karawita, C., and Jacobson, D. A., "A procedure to study sub-synchronous interactions in wind integrated power systems," *IEEE Trans. Power Syst.*, Vol. 28, No. 1, pp. 377–384, February 2013.

[18] Irwin, G. D., Jindal, A. K., and Isaacs, A. L., "Sub-synchronous control interactions between type 3 wind turbines and series compensated AC transmission systems," *2011 IEEE Power and Energy Society General Meeting*, Paper no. 12303463, pp. 1–6, San Diego, CA, 24–29 July 2011.

[19] Suriyaarachchi, D. H. R., Annakkage, U. D., Karawita, C., Kell, D., Mendis, R., and Chopra, R., "Application of an SVC to damp sub-synchronous interaction between wind farms and series compensated transmission lines," *2012 IEEE Power and Energy Society General Meeting*, Paper no. 13170150, pp. 1–6, San Diego, CA, 22–26 July 2012.

[20] Karaagac, U., Faried, S. O., Mahseredjian, J., and Edris, A.-A., "Coordinated control of wind energy conversion systems for mitigating subsynchronous interaction in DFIG-based wind farms," *IEEE Trans. Smart Grid*, Vol. 5, No. 5, pp. 2440–2449, September 2014.

[21] Leon, A. E., and Solsona, J. A., "Sub-synchronous interaction damping control for DFIG wind turbines," *IEEE Trans. Power Syst.*, Vol. 30, No. 1, pp. 419–428, January 2015.

[22] Huang, P.-H., El Moursi, M. S., Xiao, W., and Kirtley, J. L., "Subsynchronous resonance mitigation for series-compensated DFIG-based wind farm by using two-degree-of-freedom control strategy," *IEEE Trans. Power Syst.*, Vol. 30, No. 3, pp. 1442–1454, May 2015.

[23] Wang, L., Xie, X., Jiang, Q., Liu, H., Li, Y., and Liu, H., "Investigation of SSR in practical DFIG-based wind farms connected to a series-compensated power system," *IEEE Trans. Power Syst.*, Vol. 30, No. 5, pp. 2772–2779, September 2015.

[24] Shao, S., Abdi, E., Barati, F., and McMahon, R., "Stator-flux-oriented vector control for brushless doubly fed induction generator," *IEEE Trans. Ind. Electron.*, Vol. 56, No. 10, pp. 4220–4228, October 2009.

[25] Ostadi, A., Yazdani, A., and Varma, R. K., "Modeling and stability analysis of a DFIG-based wind-power generator interfaced with a series-compensated line," *IEEE Trans. Power Del.*, Vol. 24, No. 3, pp. 1504–1514, July 2009.

BIOGRAPHIES

Jian Zhang received his Ph.D. in electrical engineering from North China Electric Power University, Beijing, China, in 2014. He was then a research scholar at the University of Connecticut, Storrs, CT, USA, from November 2013 to October 2014. Currently he is a postdoctor in control and computer engineering at North China Electric Power University. His research interests include power system SSO, power electronics, and microgrids.

Xiangning Xiao received his M.E. in electrical engineering from North China Electric Power University, Beijing, China, in 1981. Currently he is a professor of electrical engineering at North China Electric Power University. His research interests include power electronics in power grids with new energy resources, power quality and its improvement in power systems, as well as power system subsynchronous oscillation.

Peng Zhang received his Ph.D. in electrical engineering from University of British Columbia, Vancouver, BC, Canada. He is an assistant professor of electrical engineering at the University of Connecticut, Storrs, USA. He was a system planning engineer at British Columbia Hydro and Power Authority (2006–2010), where he planned and designed seven large wind farms. His recent efforts have led to the creation of UConn's frst photovoltaic array, a study for hardening Eversource Energy power infrastructure against extreme weathers, a Building Innovator Award from U.S. DOE, and a design of University of Connecticut's Depot Campus Microgrid. He is a registered professional engineer in British Columbia, Canada, and an editor of *Electric Power Components and Systems*. His research interests include active distribution grids, grid resilience and reliability under high penetration of renewables, networked microgrids, and smart oceanw technologies.

Jingjing Lu received her B.E. in electrical engineering from North China Electric Power University, Beijing, China, in 2010. Currently she is a Ph.D. student at North China Electric Power University. Her research interests include power quality and its improvement, power electronics, and microgrids.

Taofeek Orekan received his B.Sc. in electrical engineering from Southern Polytechnic State University, Atlanta, GA, USA. He is currently working toward his Ph.D. at University of Connecticut, Storrs, USA. His research interests include dynamic modeling of ocean energy systems and the design and testing of point absorber wave energy converters (WECs) with a focus on improving reliability and power-quality issues.